Article:
Auer, S (2015) Nucleation of polymorphic amyloid fibrils. Biophysical Journal, 108 (5). 1176 - 1186. ISSN 0006-3495

https://doi.org/10.1016/j.bpj.2015.01.013

Nucleation of polymorphic amyloid fibrils

Stefan Auer

School of Chemistry, University of Leeds, Leeds LS2 9JT, United Kingdom

*Correspondence: s.auer@leeds.ac.uk

ABSTRACT

One and the same protein can self-assemble into amyloid fibrils with different morphologies. The phenomenon of fibril polymorphism is relevant biologically, because different fibril polymorphs can have different toxicity, but a predictive tool for which polymorph forms and under what conditions is absent. Here we consider the nucleation of polymorphic amyloid fibrils occurring by direct polymerization of monomeric proteins into fibrils and treat it within the framework of our newly developed non-standard nucleation theory, which allows the prediction of the concentration dependence of the nucleation rate for different fibril polymorphs. The results obtained highlight that the concentration dependence of the nucleation rate is closely linked with the protein solubility and a threshold monomer concentration below which fibril formation becomes biologically irrelevant. The presented relation between the nucleation rate, the fibril solubility, the threshold concentration and the binding energies of the fibril building blocks within fibrils might prove a valuable tool to design new experiments to control the formation of particular fibril polymorphs.

Keywords: Amyloid fibrils, polymorphism, nucleation theory, protein aggregation

INTRODUCTION

The structure and mechanism of formation of amyloid fibrils is being widely researched, not only because they are involved in many human diseases (1), but also due to the variety of applications as novel biomaterials in nanoscience (2). Although amyloid fibrils share a common cross-β-structure formed by intertwined layers of β-sheets extending in direction parallel to the fibril axis (3), the conformation and the stacking of the β-strands in β-sheets can differ in fibrils of the same protein, a phenomenon known as fibril polymorphism (4-6). For example stacking polymorphism of fibrils has been observed in microcrystals of short hexapeptides where β-strands within β-sheets can arrange parallel or anti-parallel, and the orientation and stacking of β-sheets can differ (7). The stacking of β-sheets in fibrils can also lead to differences in the fibril thickness which in turn can lead to differences in their twisting behaviour and helical pitch as has been shown for fragments of Bovine serum albumin (8) and the TTR peptide (9). A well known example for conformational polymorphism are fibrils of the amyloid β (Aβ) peptide associated with Alzheimer's disease that have several distinct morphologies including the ones where the β-strand in the fibril adopt an extended or a hairpin conformation (10, 11). The Aβ fibrils also exhibit packing polymorphism where the molecules are in the same conformation but pack in the fibril with different stacking or symmetry (11-13). Fibrils of numerous other proteins also show polymorphism including α-synuclei

(14), yeast and mammalian prion proteins (15, 16), and insulin (17) (see Refs. (4-6, 18) for a more complete list). The biological relevance of amyloid fibril polymorphism comes from the observation that the toxicity of polymorphs can differ (see e.g. Refs. (11, 19)). A prominent example is strain polymorphism and species barriers in prions. In this phenomenon, the prion protein can propagate multiple strains (fibril structures) each of which results in a different pathology. Propagation is sequence dependent, which prevents prion transmission between related species (see e.g. Refs. (15, 20, 21)). The conditions under which fibril polymorphism can be observed are manifold. The fibril morphology depends on intrinsic factors such as the protein amino acid sequence, and it has been observed that a single point mutation can switch the fibril morphology from predominately parallel to predominately antiparallel (22). It also depends on solution conditions (pH value (23), salts (24)) and other external factors (temperature (25), quiescent or agitated (11), seeds (26)), but even under the same conditions variations in the fibril morphology exist (27).

The mechanism of how polymorphic amyloid fibrils form and under which conditions is subject of intense research (4-6). It is generally accepted that amyloid fibrils form by a nucleation and growth mechanism (e.g. Refs. (28-30)). The nucleation of amyloid fibrils refers to the process of random generation of nanofibrils that have the ability to grow irreversibly. Unless the nanofibril size exceeds the size of the nucleus, the nanofibril is more likely to dissolve than to grow. Depending on the solution conditions amyloid fibrils nucleate in one step (directly from the solution) or in two steps (step one being the appearance of nonfibrillar oligomers in the solution and step two being the oligomer conversion into fibrils) (31). In analogy to crystal nucleation where the structure of the nucleus determines the structure of the bulk solid, the structure of the fibril nucleus might determine the structure of the fibril formed in the solution. This implies that every fibril polymorph requires a distinct nucleation event and certain nucleation events may occur more frequently than others. Amyloid fibril growth refers to the process of addition of monomers to either the fibril ends or fibril surfaces leading to fibril lengthening and thickening, respectively. During growth the fibrils can be affected by other processes such as fibril fragmentation (11, 28), fibril coalescence, Ostwald ripening and secondary nucleation events such as the nucleation of fibrils on the surface of existing ones (32). Although a common feature of fibril polymorphism is that they are self-propagating, such growth effects can also lead to the formation of fibril polymorphs or determine which polymorph dominates. For example, fibril coalescence and Ostwald ripening can lead to fibrils with different thickness, and thus different twisting behaviour and helical pitch, as in the case of Bovine serum albumin (8) and the TTR peptide (9) mentioned above. It has also been shown that the fragmentation rate is the reason that Aβ40 fibril with two-fold symmetry form in agitated solutions and Aβ40 fibrils with three-fold symmetry form in absence of shear (11).

In order to better understand why and how polymorphic amyloid fibrils form and under which conditions, it is necessary to develop a theoretical model of their formation. Models based on the protein physicochemical properties have been developed to predict the aggregation propensities but they are unable to differentiate between polymorphic fibril structures (33-36). Similarly, models on the molecular level based on rate equations have been used to analyse protein fibrillation experiments (28, 37, 38), but they are also unable to differentiate between polymorphic fibril structures because they work with a fixed fibril shape. Various Molecular Dynamic (MD) simulation studies using a full atomistic description of proteins have been reported that investigate fibril polymorphism (39-43), but at

present they are restricted to calculations of the thermodynamic stability of fibrils composed of short peptide fragments. Using a simplified protein model it has been possible to perform MD simulations, which show that one protein can self-assemble into different fibril morphologies, and that their formation can be kinetically (rather than thermodynamically) controlled (44).

Here we approach the problem by considering the nucleation of amyloid fibrils into polymorphic structures when the process occurs in one step by a direct polymerization of monomers into fibrils. Two-step nucleation of polymorphic fibrils, and fibril polymorphism that occurs during fibril growth, or is determined by fibril growth, are not considered. Recently, our simulations have shown that amyloid fibril nucleation occurring by a direct polymerization of monomers is a peculiar kind of nucleation not complying with standard nucleation theory (45, 46), because the concept of the existence of a critical nucleus breaks down (the nucleus size does not have a unique value) and there exist jumps in the nucleation rate of many orders of magnitude at certain concentrations (47, 48). This called for the development of a new description of amyloid fibril nucleation which is able to describe this non-standard nucleation of amyloid fibrils (30, 49). The objective of this article is to apply this new nucleation model to the phenomenon of amyloid fibril polymorphism, and to predict how the fibril solubility, the threshold concentration below which fibril formation becomes biologically irrelevant, and the nucleation rate is affected by changes in the conformation and the stacking of the fibril building blocks (the β-strands) or their arrangement within the fibril. Our considerations of fibril polymorphism pertain to changes in (i) the β-strand length associated with the onset of polyglutamine disorders (50), (ii) the conformation of the β-strand from extended to a hairpin reported for Aβ_{40} (10), (iii) the parallel and anti-parallel stacking of β-strands in β-sheets as observed in short peptides and natural proteins (7, 22), (iv) and the asymmetry in the hydrophobicity between the two β-sheet surfaces that can lead to different stacking of β-sheets in fibrils (7). The emphasis of this work is to reveal general rules that underlie the nucleation of one and the same protein into different fibril polymorphs, to provide conceptual insight into factors that can tip the nucleation process in favour of one or another fibril polymorph. For this reason we will apply our theoretical framework to a model peptide rather than to a specific protein.

MATERIALS AND METHODS

Model

In our model (30, 49, 51), each β-strand (a segment of a protein chain composed of typically up to ten amino acids) is represented by a right rectangular prism (Figure 1).

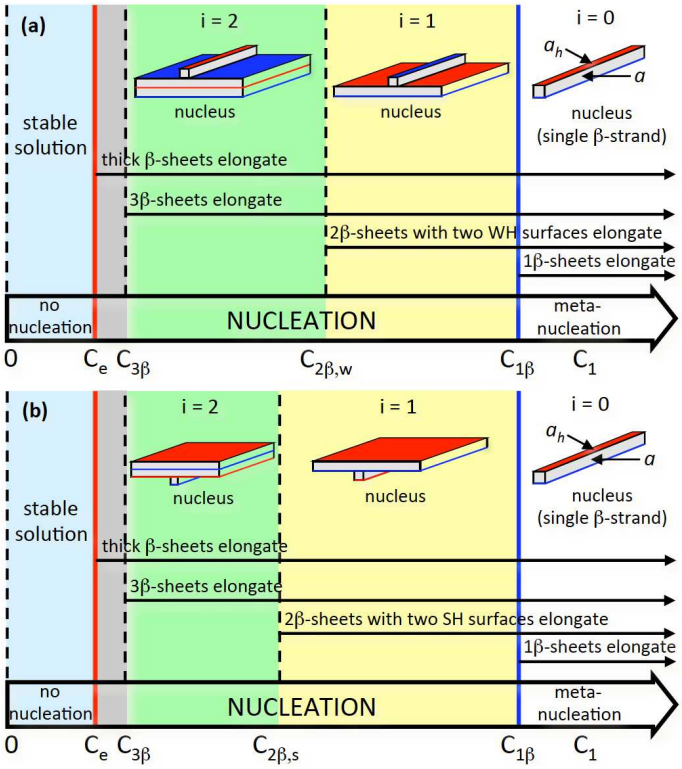

Figure 1. Phase diagram for fibrils composed of β-strands with one WH (blue) and a SH (red) side. The fibril solubility C_e indicates the concentration ranges in which the protein solution is in stable ($0 \le C_1 \le C_e$) or metastable ($C_1 > C_e$) thermodynamic equilibrium at a given temperature. **(a)** In the metanucleation range ($i = 0$) the nucleus is a single β-strand. In the first ($i = 1$) nucleation range a 2β-sheet with two WH surfaces can elongate and the nucleus is a 1β-sheet with one β-strand attached with its SH side to the SH 1β-sheet surface. Similarly, in the second ($i = 2$) nucleation range a 3β-sheet with one SH and one WH surface can elongate and the nucleus is a 2β-sheet with one β-strand attached with its WH side to the weak 2β-sheet surface. **(b)** As in (a), but in the first ($i = 1$) and second ($i = 2$) nucleation ranges the fibril nuclei are a 1β and 2β-sheet (with two SH surfaces) with one β-strand attached to its WH and SH side, respectively.

Due to their strong hydrogen bonds, the β-strands can arrange themselves laterally into β-sheets. The sheets consist of different number m of β-strands ($m = 1,2,3,...$) and are parallel to the fibril lengthening axis. Along its thickening axis the fibril is built up of $i\beta$-sheets ($i = 1,2,3,...$) which are held together by e.g. relatively weak hydrophobicity-mediated bonds between the β-strands. Because the orientation of side-chains within a β-strand alternates, the hydrophobicity of the two β-sheet surfaces is generally different. In our model (49) we assume that for a 1β-sheet, i.e. a single β-sheet, the strongly hydrophobic (SH) surface is always on top (as indicated by the red surface/line in Figure 1) whereas the weakly hydrophobic (WH) surface is at the bottom (as indicated by the blue surface/line in Figure 1). In addition, a β-strand can only bind to a WH β-sheet surface with its WH side (blue binds to blue) and to an SH β-sheet surface with its SH side (red binds to red). Thus, the hydrophobicity of the surface of a nanofibril alternates with increasing number of β-sheets (red, blue, red,

blue, etc.). Since the fibril width is fixed and equal to the β-strand length, the fibril can be considered as a 2D aggregate in the *m*,*i* plane, with building blocks (the β-strands) arranged in a 2D lattice with simple rectangular symmetry.

Essential parameters in our theory to describe the ontogenesis of the smallest nanosized amyloid fibrils are the dimensionless specific surface energies $\psi = a\sigma / kT = E / 2kT$ and $\psi_w = a_h\sigma_w / kT = E_w / 2kT$, $\psi_s = a_h\sigma_s / kT = E_s / 2kT$ of the fibril faces perpendicular to the lengthening *m* axis and the thickening *i* axis, respectively. The σ's are the dimensional specific surface energies of the fibril surfaces, the *a*'s are the areas of the β-strand faces (Figure 1), *k* is the Boltzmann constant, and *T* is the absolute temperature. The second equality in these equations results from using the approximate relations $\sigma = E / 2a$, $\sigma_s = E_s / 2a_h$ and $\sigma_w = E_w / 2a_h$ between the σ's and the binding energies *E*'s between nearest neighbour β-strands (52).

In order to model conformational polymorphism of β-strands within fibrils, it is necessary to introduce the binding energies ε and ε_s , ε_w between nearest-neighbour amino acid due to hydrogen bonding, and to strong and weak hydrophobic bonding, respectively. Although our model can be applied to hetero polypeptides, for simplicity, in this work we only consider homo polypeptides for which the binding energies between amino acids in neighbouring β-strands are the same. Then the *E*'s can be written as $E = n\varepsilon$, $E_s = n_s\varepsilon_s$ and $E_w = n_w\varepsilon_w$, where *n* is the number of amino acids between two nearest-neighbour β-strands in a β-sheet that form hydrogen bonds, and n_s, n_w are the number of amino acids that form strong and weak hydrophobic bonds between nearest neighbour β-strands in successive β-sheets, respectively. The dimensionless specific surface energies ψ_s and ψ_w can then be written as

$$\psi_s = n_s\alpha_s \quad (1)$$

$$\psi_w = n_w\alpha_w \quad (2)$$

where $\alpha_s = \varepsilon_s / 2kT$ and $\alpha_w = \varepsilon_w / 2kT$ are the dimensionless specific surface energies per amino acid due to strong and weak hydrophobic bonds, respectively.

Importantly, the dimensionless specific surface energy ψ can contain contributions from both nearest-neighbor hydrogen bonding and hydrophobicity-mediated bonds and is given by

$$\psi = n\alpha + c_s n_s\alpha_s + c_w n_w\alpha_w \quad (3)$$

where $\alpha = \varepsilon / 2kT$ is the dimensionless specific surface energies per amino acid due to hydrogen bonds, and c_s, c_w are parameters determining the contributions of the strong and weak hydrophobicity-mediated bonds to ψ . For our illustrations we set $c_s = c_w = 0.5$, which means that the contribution of the strength of the hydrophobicity mediated bonds to ψ is taken to be the average of the weak and strong hydrophobic surfaces.

To calculate ψ_s, ψ_w and ψ for hetero polypeptides, the binding energies between amino acids pairs needs to be know, so that the dimensionless specific surface energies can be calculated by summation over amino acids pairs in neighbouring β-strands (53).

Phase diagram

A prerequisite for the application of nucleation theory to the formation of new phases is the understanding of the thermodynamic phase diagram. Experiments with different fibril polymorphs of Aβ40 show that their solubility differs (13, 54). Both theoretical considerations (30, 49, 51) and a computer-simulated peptide solubility diagram (55, 56) reveal that for the irreversible elongation of differently thick amyloid fibrils thermodynamics requires different ranges of the concentration C_1 of monomeric β-strands (peptides or protein segments) in the solution. Figure 1 illustrates schematically these ranges at a fixed absolute temperature T at which the β-strands are in practically fully extended conformation. These ranges are limited by the equilibrium concentration (or solubility) C_e of the bulk fibrillar phase and the equilibrium concentrations (or solubilities) $C_{1\beta}$, $C_{2\beta,w}$, $C_{2\beta,s}$, $C_{3\beta}$, etc. of the fibrils constituted of one β-sheet, two equally long β-sheets with two WH or two SH surfaces, three equally long β-sheets, etc., respectively. The solubilities are merely the C_1 values at which the respective iβ-sheets, i.e. fibrils built up of i β-sheets, neither lengthen nor dissolve. The iβ-sheets with an odd number i of layers have always one WH and one SH surface and their solubility $C_{i\beta}$ is related to C_e by the expression (49) ($i = 1,3,5,...$)

$$C_{i\beta} = C_e \exp\left[(\psi_w + \psi_s)/i\right] \tag{4}$$

The existence of two solubility values for iβ-sheets with an even number i of layers is due to the fact that they can have either two WH or two SH surfaces, respectively, and their solubilities $C_{i\beta,w}$ and $C_{i\beta,s}$ are related to C_e and by the expressions (49) ($i = 2,4,6,...$)

$$C_{i\beta,w} = C_e \exp(2\psi_w / i) \tag{5}$$

$$C_{i\beta,s} = C_e \exp(2\psi_s / i) \tag{6}$$

In this work, we mostly consider the symmetric case when the hydrophobicity of both β-strand surfaces is the same, i.e. $\psi_w = \psi_s \equiv \psi_h$, then the three equations above simplify to one (51) ($i = 1,\ 2,\ 3,\ \ldots$)

$$C_{i\beta} = C_{i\beta,w} = C_{i\beta,s} = C_e \exp(2\psi_h / i) \tag{7}$$

As indicated in Figure 1, the $C_1 > C_{1\beta}$ range (range $i = 0$ in the figure) corresponds to metanucleation, a process of fibril formation without energy barrier, because then each protein monomer (i.e. single β-strand) in the solution acts as fibril nucleus as attachment of another monomer to it allows irreversible elongation. When $C_1 > C_{2\beta,w}$, 2β-sheets with two weak hydrophobic surfaces can lengthen irreversibly. Importantly, in the $C_{2\beta,w} < C_1 < C_{1\beta}$ range (range $i = 1$ in Figure 1) the 1β-sheets tend to dissolve and their appearance is due to fluctuations. In this range the fibril nucleus is a 1β-sheet plus one β-strand attached with its SH side to the SH 1β-sheet side so that a fibril prenucleus is any of the randomly formed, differently long 1β-sheets in the solution. When $C_1 > C_{2\beta,s}$, also the 2β-sheets with two strong hydrophobic surfaces can lengthen irreversibly, and in the $C_{2\beta,s} < C_1 < C_{1\beta}$ range (range $i = 1$ in Figure 1) the corresponding fibril nucleus is a 1β-sheet plus one β-strand attached with its WH side to the WH 1β-sheet side (see Figure 1). The situation is analogous with the 3β-sheets when $C_1 > C_{3\beta}$, because then these sheets can elongate irreversibly, and in the $C_{3\beta} < C_1 < C_{2\beta w}$ or $C_{3\beta} < C_1 < C_{2\beta s}$ ranges (range $i = 2$ in Figure 1), the fibril nucleus is a 2β-sheet with one β-strand attached sidewise.

The general rules are, therefore, that in the *i*th supersaturation range, defined by (49) ($i = 1,\ 3,\ 5,\ \ldots$)

$$C_e \exp\left[2\psi_w/(i+1)\right] < C_1 < C_e \exp\left[(\psi_w+\psi_s)/i\right] \quad (8)$$

$$C_e \exp\left[2\psi_s/(i+1)\right] < C_1 < C_e \exp\left[(\psi_w+\psi_s)/i\right] \quad (9)$$

the fibril nuclei are composed of an odd number i of β-sheets plus one β-strand attached to the SH or WH side, respectively (Figure 1). In these ranges, all different length $i\beta$-sheets are fibril prenuclei, and these sheets plus one $i\beta$-strand attached to the WH or SH surface, are the fibril nuclei for the $(i+1)\beta$-sheet-thick fibrils with either two WH or SH sides that can lengthen irreversibly. Similarly, in the *i*th supersaturation range, defined by ($i = 2,\ 4,\ 6,\ \ldots$)

$$C_e \exp\left[(\psi_w+\psi_s)/(i+1)\right] < C_1 < C_e \exp(2\psi_w/i) \quad (10)$$

$$C_e \exp\left[(\psi_w+\psi_s)/(i+1)\right] < C_1 < C_e \exp(2\psi_s/i) \quad (11)$$

the fibril nuclei are composed of an even number i of β-sheets plus one β-strand attached to the SH or WH side, respectively (Figure 1). For the symmetric case (then $\psi_s = \psi_w \equiv \psi_h$), the four equations above simplify to one general rule that in the ranges (51) ($i = 0,\ 1,\ 2,\ 3,\ \ldots$)

$$C_e \exp\left[2\psi_h/(i+1)\right] < C_1 < C_e \exp(2\psi_h/i) \quad (12)$$

all differently long $i\beta$-sheets are fibril prenuclei, and these sheets plus one β-strand attached to one of their two sides are the nuclei of the $(i+1)\beta$-sheet-thick fibrils that can lengthen irreversibly.

Nucleation rate

Which fibrils form in a protein solution, and how fast, is determined by the nucleation rate J ($m^{-3}\ s^{-1}$). Experiments on protein aggregation are often performed at fixed temperature T, and based on the phase diagram discussed above we can write down expressions for J in the nucleation and metanucleation ranges. The concentration dependence of the nucleation rate in the metanucleation range (range $i = 0$ in Figure 1) in which each monomer in the solution acts as fibril nucleus is given by (49) ($C_1 > C_{1\beta}$)

$$J = A_1 C_1^2 (1 - A_2 C_1^{-1}) \quad (13)$$

where $A_1 = 2k_e/C_e$, $A_2 = C_e \exp(\psi_w + \psi_s)$, k_e is the attachment frequency of monomers to one of the two hydrogen-bond sides of a given monomer at equilibrium, C_e is the fibril solubility, and the threshold concentration $C_{1\beta}$, given by

$$C_{1\beta} = C_e \exp(\psi_s + \psi_w) \quad (14)$$

is obtained from eq (4) with $i = 1$. For the symmetric case (then $\psi_s = \psi_w \equiv \psi_h$), the constants simplify to (30): $A_1 = 2k_e/C_e$, $A_2 = C_e \exp(2\psi_h)$ and $C_{1\beta} = C_e \exp(2\psi_h)$.

The formula for J in the *i*th nucleation range when the fibril nuclei are composed of an odd number ($i = 1,\ 3,\ 5,\ \ldots$) of β-sheets plus one β-strand (corresponding to supersaturation ranges $i = 1,\ 3,\ 5,\ \ldots$) is given by (49)

$$J = A_1 C_1^{i+2} \frac{1 - A_2 C_1^{-1}}{\left(1 - A_3 C_1^{i}\right)^2} \quad (15)$$

with $A_1 = (2k_e/C_e^{i+1})\exp(-2\psi i - \psi_w + \psi_s)$ and $A_2 = C_e \exp\left[2\psi_w/(i+1)\right]$ (for $C_e \exp\left[2\psi_w/(i+1)\right] < C_1 < C_e \exp\left[(\psi_w+\psi_s)/i\right]$) or

$A_1 = (2k_e / C_e^{i+1})\exp(-2\psi i - \psi_s + \psi_w)$ and $A_2 = C_e \exp\left[2\psi_s/(i+1)\right]$ (for $C_e \exp\left[2\psi_s/(i+1)\right] < C_1 < C_e \exp\left[(\psi_w + \psi_s)/i\right]$ when the β-strand is on the nucleus SH or WH side, respectively. The constant A_3 is given by $A_3 = C_e^{-i} \exp\left[-(\psi_w + \psi_s)\right]$ in both cases.

When the fibril nuclei are composed of an even number $i = 2, 4, 6, ...$ of β-sheets plus one β-strand (supersaturation ranges $i = 2$, 4, 6, …), the fibril nucleation rate is given again by eq (15), but with $A_1 = (4k_e / C_e^{i+1})\exp(-2\psi i)$ and $A_2 = C_e \exp\left[(\psi_w + \psi_s)/(i+1)\right]$. As to the constant A_3, it is given by $A_3 = C_e^{-i} \exp(-2\psi_w)$ (for $C_e \exp\left[(\psi_w + \psi_s)/(i+1)\right] < C_1 < C_e \exp(2\psi_w / i)$) when the β-strand is on one of the prenucleus two WH sides, or by $A_3 = C_e^{-i} \exp(-2\psi_s)$ (for $C_e \exp\left[(\psi_w + \psi_s)/(i+1)\right] < C_1 < C_e \exp(2\psi_s / i)$) when the β-strand is on one of the nucleus two SH sides. For the symmetric case, the fibril nucleation rate is given again by eq (15), but with $A_1 = (4k_e / C_e^{i+1})\exp(-2\psi i)$, $A_2 = C_e \exp\left[2\psi_h/(i+1)\right]$, and $A_3 = C_e^{-i} \exp(-2\psi_h)$ in the supersaturation ranges specified by eq (12).

Fibril solubility

Different fibril polymorphs will have different solubilities (13, 54). As the effect of changing molecular interactions between β-strand on C_e is not always known experimentally, we estimate it theoretically by making use of the van't Hoff equation and the Haas-Drenth lattice model (57) for protein crystals. The integrated van't Hoff equation is given by $C_e = C_r \exp(-\lambda)$ where C_r is a practically temperature independent reference concentration and $\lambda = L / kT$ is the dimensionless latent heat of peptide aggregation into β-sheets. Here L is the latent heat of peptide aggregation into such aggregates. In the Haas-Drenth lattice model (57) for protein crystals λ is half the dimensionless binding energy of peptides in the aggregates, which is equivalent to the dimensionless broken bond energy $\lambda = 2\psi + \psi_s + \psi_w$ at the periphery of a fibril in the m,i plane. The fibril solubility is then given by

$$C_e = C_r \exp\left(-2\psi - \psi_s - \psi_w\right) \qquad (16)$$

and simplifies to $C_e = C_r \exp\left[-2(\psi + \psi_h)\right]$ in the symmetric case.

RESULTS

The recipe to apply our newly developed non-standard nucleation theory to predict the $J(C_1)$ dependence for different fibril polymorphs is as follows: (1) Calculation of the dimensionless specific surface energies ψ_s, ψ_w and ψ for different fibril polymorphs from eqs 1 to 3. This requires the knowledge of the conformation of the β-strands in the fibril as they define the number n of bonds between amino acids, and the associated binding energies between them. (2) Calculation of the fibril solubility C_e for different fibril polymorphs from eq 16. This requires the knowledge of C_e for one fibril polymorph that serves as a reference structure. (3) Calculation of the $J(C_1)$ dependence from eqs 13 to 15, which requires knowledge of the elongation rate k_e. We apply this recipe to the fibril polymorphs illustrated in Figure 2. As already

mentioned in the introduction, the emphasis of this work is to provide conceptual insight into factors can tip the nucleation process in favour of one or another fibril polymorph. For this reason we will apply our theoretical framework to a model peptide rather than to a specific protein.

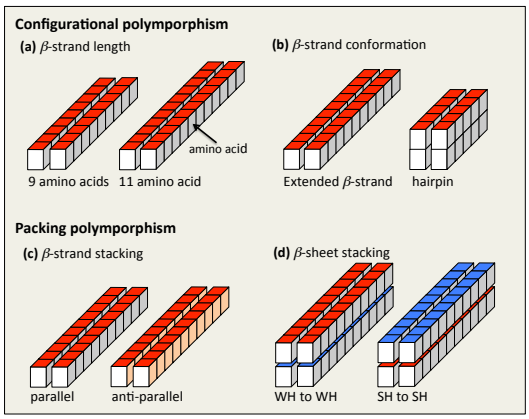

Figure 2. Illustration of fibril polymorphs considered in this work. Conformational polymorphism where the fibril polymorphs are composed of extended β-strand of different lengths (9 or 11 amino acids) **(a)**, and β-strands in an extended or hairpin conformation **(b)**. Stacking polymorphism where the fibril polymorphs are composed of extended β-strands that stack either parallel or anti-parallel in β-sheets **(c)**, and β-sheets that stack either by binding with their two WH or two SW surfaces **(d)**. The red and blue surfaces indicate the SH and WH β-strand sides, respectively. The light grey and light orange surfaces indicate the strong and weak hydrogen bonding β-strand sides, respectively.

Conformational polymorphism

Perhaps the simplest example of conformational polymorphism is where the number of amino acids of the β-strands within a fibril differs. The β-strand length is relevant because it has been associated with polyglutamine disorders (50). Polyglutamine disorders are a class of nine neurodegenerative disorders including Huntington's disease associated with the aggregation of polyglutamine repeats. The hallmark feature of these diseases is that the onset of the disease correlates with the length of the polyglutamine repeats. The aggregation and pathologies are typically observed above a threshold of 35-40 repeats, and the longer the repeat the sooner the symptoms appear (50, 58). In order to illustrate the effect of the β-strand length on the $J(C_1)$ dependence we consider β-strands composed of 9, 10 and 11 amino acids (Figure 2a) that assemble in their fully extended conformation in a nanosized amyloid fibril. Step (1) of the recipe is to determine the dimensionless specific surface energies. As the structure of the β-strands in the fibril is fully extended, the number n of amino acids that form hydrogen bonds between two-nearest neighbour β-strands in a β-sheet and the numbers n_w, n_s of amino acids that form hydrophobic bonds between two-nearest neighbour β-strands are the same and given by $n = n_s = n_w = 9$, 10 and 11 for β-strands of length 9, 10, and 11, respectively. Assuming that the dimensionless specific surface energy per amino acid due to hydrogen-bonding is $\alpha = 1$ (corresponding to $\varepsilon = 2\,kT$, a value in the range of hydrogen bonding energies measured experimentally

(59)), that the ones due to strong and weak hydrophobic bonds are $\alpha_s = \alpha_w = 0.1$ (corresponding to $\varepsilon_s = \varepsilon_w = 0.2\,kT$, a value typically used in protein simulations (60)), and that the parameter $c_s = c_w = 0.5$, the values for the dimensionless specific surface energies are obtained from eqs 1 to 3 and given by $\psi = 9.9$, $\psi_s = \psi_w = \psi_h = 0.9$ for β-strands of length 9, $\psi = 11$, $\psi_s = \psi_w = \psi_h = 1$ for β-strands of length 10, and by $\psi = 12.1$, $\psi_s = \psi_w = \psi_h = 1.1$ for β-strands of length 11. These ψ values are in the range of values estimated for short fibrils (31, 56). Step (2) of the recipe is to calculate of the fibril solubility C_e for different fibril polymorphs. Assuming that the fibril solubility for fibrils composed of β-strands with 10 amino acids is $C_e = 6.0 \times 10^{21}$ m^{-3} (= 10 μM) (e.g. ref (61)), we calculate from eq 16 that $C_r = 1.6 \times 10^{32}$ m^{-3}. Importantly, as the binding energies of β-strands with different lengths within the fibrils are different, their fibril solubilities are different (see methods). Assuming that $C_r = 1.6 \times 10^{32}$ m^{-3} is independent of the length, and substituting C_r and the ψ, ψ_h values above in eq 16, the solubilities for fibrils composed of peptides composed of 9 and 11 amino acids are $C_e = 6.62 \times 10^{22}$ m^{-3} (= 110 μM) and $C_e = 5.41 \times 10^{21}$ m^{-3} (= 0.9 μM), respectively. Figure 3a illustrates the so obtained (exponential) decrease of C_e with increasing length (eq 16).

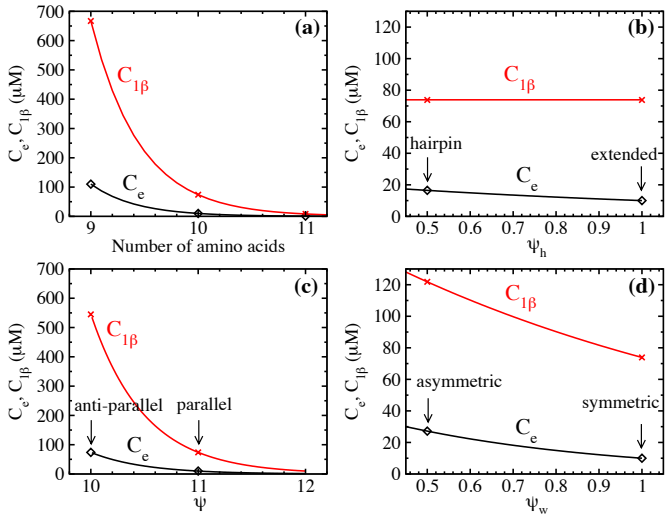

Figure 3. Solubility C_e (diamonds) and threshold concentration $C_{1\beta}$ (crosses) of fibrils composed of (a) extended β-strands of length 9, 10 and 11 amino acids. The corresponding values for the dimensionless surface energies are $\psi_h = 0.9$, 1, 1.1 and $\psi = 9.9$, 11, 12.1 for length 9, 10, and 11, respectively. (b) extended β-strands and β-strands in a hairpin conformation. The corresponding surface energies are $\psi =$ 11 (for both) and $\psi_h = 1$ (extended) or 0.5 (hairpin). (c) extended β-strands arranged parallel and anti-parallel. The corresponding surface energies are $\psi_h = 1$ (for both) and $\psi = 10$ (anti-parallel) or 11 (parallel). (d) extended β-strands with asymmetric hydrophobic surfaces between β-sheets. The corresponding values for the dimensionless surface energies are $\psi_s = 1$ (for all) and $\psi = 11$, 10.75 and $\psi_w = 1$, 0.5 for the symmetric and

the asymmetric hydrophobic surfaces, respectively. In all panels the solid red and black lines are obtained from equations (14) and (16), respectively.

Step (3) of the recipe is to calculate the $J(C_1)$ dependence for the different fibril polymorphs. Using a typical value for the fibril elongation rate $k_e = 10^{-4}$ s^{-1} (e.g. ref (28)), and assuming that it is independent of the length, allows us to calculate the $J(C_1)$ dependence from eqs 13 to 15 with the A's for the symmetric case (because $\psi_s = \psi_w = \psi_h$). As can be seen in Figure 4a, the characteristic feature of the $J(C_1)$ dependence is the sharp rise at the transition concentrations $C_{i\beta}$ over a very narrow concentration range; 7 orders of magnitude at the nucleation/metanucleation border $C_{1\beta}$ and even more at $C_{2\beta}$. As mentioned in the introduction, such a sharp rise in the nucleation rate is a peculiar kind of nucleation and does not comply with standard nucleation theory (30). The importance of $C_{1\beta}$ comes from the fact that it appears as a threshold concentration below which fibril formation becomes biologically irrelevant, because only one fibril can be nucleated within a day in volumes of about 1 μm^3 or smaller, comparable to that of a cell.

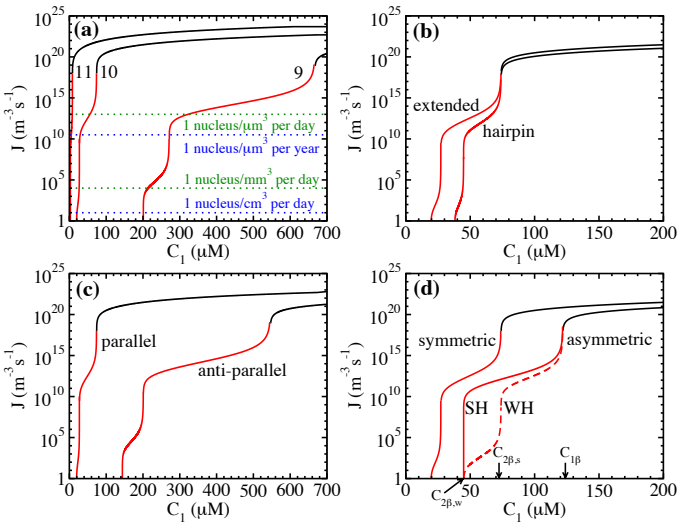

Figure 4. Concentration dependence of the nucleation rate J for fibrils composed of (a) extended β-strands of length 9, 10 and 11 amino acids (as indicated). (b) extended β-strands and β-strands in a hairpin conformation (as indicated). (c) extended β-strands arranged parallel and anti-parallel (as indicated). (d) extended β-strands with symmetric and asymmetric hydrophobic surfaces between β-sheets as indicated. In the asymmetric case the label WH and SH indicate the nucleation rate where the fibril nuclei is a 1β-sheet plus one β-strand attached to the SH and WH side of the sheet, respectively. The corresponding values for the dimensionless surface energies are as in Figure 3. In all cases, the black and red lines indicate the rate in the metanucleation and nucleation ranges, respectively.

Figure 4a also shows that the main effect of increasing the β-strand length on the $J(C_1)$ dependence is to shift $C_{1\beta}$ to lower concentrations and to promote protein fibrillation, because metanucleation commences at lower C_1 values. Using the C_e

values calculated above in eq 14, the threshold concentrations for fibrils with 9, 10 and 11 amino acids are $C_{1\beta} = 4.0 \times 10^{23}$ m^{-3} (= 665.5 μM), $C_{1\beta} = 4.4 \times 10^{22}$ m^{-3} (= 73.8 μM), and $C_{1\beta} = 4.9 \times 10^{21}$ m^{-3} (= 8.1 μM), respectively (Figure 3a). The dependence of $C_{1\beta}$ on C_e (eq 14), however, highlights that C_e is the determining factor in amyloid fibril nucleation and is the main reason why fibrils composed of longer β-strands nucleate faster. Even though we have considered here only a short model peptide, the prediction that the nucleation rate increases with increasing β-strand length is compatible with the experimental observation that the onset of the disease correlates with the length of the polyglutamine repeats (50).

Another example of conformational polymorphism in amyloid fibrils has been reported for the amyloid-β peptide where the Aβ_{40} peptide is in an extended and a hairpin conformation (10, 12). In order to investigate how such a change in the conformation affects the $J(C_1)$ dependence, we consider fibrils composed of β-strands with 10 amino acids in an extended conformation (as above) and a hairpin conformation (Figure 2b). The main difference for fibrils composed of β-strands in a hairpin conformation is that only half of the amino acids of the β-strand contribute to the hydrophobicity-mediated bonds between successive β-sheets and therefore $n_s = n_w = n/2 = 5$. All other parameters are the same (i.e. $\alpha = 1$, $\alpha_w = \alpha_s = 0.1$, and $c_w = c_s = 0.5$). As in the previous example, the values for the dimensionless surface energies for fibrils composed of β-strands in a hairpin conformation are obtained from eqs 1 to 3 and are given by $\psi = 11$, $\psi_s = \psi_w = \psi_h = 0.5$ (step (1) of recipe). The value $\psi = 11$ is the same for both fibril polymorphs, as the number of hydrogen and hydrophobic bonds in direction of the fibril lengthening axis is the same. Using again $C_r = 1.6 \times 10^{32}$ m^{-3} with $\psi = 11$, $\psi_h = 0.5$ in eq 16, shows that the conformational change shifts $C_e = 1.63 \times 10^{22}$ m^{-3} (= 27.1 μM) to slightly higher concentrations, see Figure 3b (step (2) of recipe). As in the previous example, we calculate the $J(C_1)$ dependence from eqs 13 to 15 with $k_e = 10^{-4}$ s^{-1} and the A's for the symmetric case (step (3) of recipe). Figure 3b shows that the main effect of this conformational change is a small decrease of $J(C_1)$ mainly because the threshold concentration $C_{1\beta} = 4.4 \times 10^{22}$ m^{-3} (= 73.8 μM) is unchanged. This can be shown by substitution of eq 16 into eq 14 which eliminates ψ_s, ψ_w in the exponents of $C_{1\beta}$, so that it only depends on ψ. Thus, the shift of C_e to slightly higher concentrations compensates the corresponding shift of $C_{1\beta}$ to lower ones. The prediction that the nucleation rates of fibrils composed of peptides in an extended β-strand and hairpin conformation differ only slightly might explain why both fibril structures have been observed experimentally (10, 12).

Packing polymorphism

We first consider packing polymorphism where β-strands within β-sheets arrange parallel or anti-parallel (Figure 2c), as it has been observed in fibrils of short peptides and natural proteins (7, 22). As before, the fibril building block is the extended β-strands composed of 10 amino acids. To distinguish between parallel and anti-parallel stacking, we assume that the hydrogen bonding energy between β-strands in a β-sheet when stacked in anti-parallel arrangement is weaker compared to when stacked

parallel. Thus, for anti-parallel stacking we set the specific surface energy per amino acid due to hydrogen bonding to $\alpha = 0.9$ which is smaller compared to $\alpha = 1$ for parallel arrangement. All other values for the model parameter are unchanged (i.e. $c_w = c_s = 0.5$ and $n_s = n_w = n = 10$). The corresponding value for the dimensionless surface energy due to hydrogen bonding for anti-parallel stacking is $\psi = 10$ (calculated as before), whereas the values for the surface energy due to hydrophobicity-mediated bonds are $\psi_s = \psi_w = \psi_h = 1$ as before (step (1) of recipe). The fibril solubility $C_e = 4.4 \times 10^{22}$ m^{-3} (= 74 μM) is obtained from eq 16 with $C_r = 1.6 \times 10^{32}$ m^{-3} (step (2) of recipe), which shows that a change in the arrangement of the β-strand in a β-sheet from parallel to anti-parallel shifts C_e to much higher concentrations (Figure 3c). Assuming again that $k_e = 10^{-4}$ s^{-1} is independent of the stacking, the $J(C_1)$ dependence is calculated from eqs 13 to 15 with the A's for the symmetric case (step (3) of recipe), illustrating that a change in the arrangement of the β-strands in a β-sheet from parallel to antiparallel shifts $C_{1\beta}$ to higher concentration and that it hampers protein fibrillation because metanucleation commences at higher C_1 values (Figure 4c). Using the C_e value calculated above in eq 14, the threshold concentration is $C_{1\beta} = 3.3 \times 10^{23}$ m^{-3} (= 545 μM) (see Figure 3c). It is worth noting that a mixture of parallel and anti-parallel fibrils in the protein solution can only be observed at concentrations in the metanucleation range of both fibrils, i.e. when $C_1 > C_{1\beta} = 545$ μM, and provided that the magnitude of the metanucleation rates are comparable and sufficiently high (see Figure 4c). Importantly, as a priory it is not known whether anti-parallel stacking decreases the specific surface energy per amino acid due to hydrogen bonding, we could also have assumed that this stacking increases it, in which case anti-parallel fibrils would nucleate faster. The general rule is, however, that increasing the specific surface energy per amino acid due to hydrogen bonding promotes protein fibrillation, and the strong effect on the $J(C_1)$ dependence might explain that a single point mutation can switch the fibril morphology from predominately parallel to predominately antiparallel (22).

Another example of packing polymorphism is when β-sheets stack differently as observed in short peptides (7). Along its thickening axis the fibril is built up of β-sheets which are held together by e.g. relatively weak hydrophobicity-mediated bonds between the β-strands. Because the orientation of side-chains within a β-strand alternates, the hydrophobicity of the two β-sheet surfaces is generally different. This asymmetry leads to fibrils that can either have two strong, two weak or one strong and one weak hydrophobic surface (Figure 2d), but which ones form? As in our previous work (49), to model the effect of asymmetry we decrease the weak specific surface tension per amino acid due to hydrophobic bonding between β-strands in consecutive β-sheets to $\alpha_w = 0.05$ while $\alpha_s = 0.1$ is kept constant. The values of all other parameter are the same as for the extended β-strand with symmetric hydrophobic surfaces (i.e $c_s = c_w = 0.5$, $n_s = n_w = n = 10$). The corresponding values for the dimensionless surface energies are obtained from equations 1 to 3 and are given by $\psi_s = 1$, $\psi_w = 0.5$, $\psi =$ 10.75 (step (1) of recipe), and the corresponding asymmetry ratio is $\psi_w / \psi_s = 0.5$. The fibril solubility is again obtained from eq 16 and is given by $C_e = 7.3 \times 10^{22}$ m^{-3} (= 27 μM) (step (2) of recipe). Thus, increasing the asymmetry (by

decreasing the asymmetry ratio) shifts C_e to higher concentrations (Figure 3d). We calculate the $J(C_1)$ dependence from eqs 13 and 15 with $k_e = 10^{-4}$ s^{-1} and the A's for the asymmetric case (step (3) of recipe). A characteristic feature in this case is, however, that in given concentration range there exist different fibril nuclei (see Figure 1). In Figure 4d we show that in the first nucleation range (range ($i = 1$) in Figure 1), the nucleation rate for fibrils where the fibril nucleus is a single β-sheet plus one β-strand attached to the SH side can be substantially higher than that where the β-strand is attached to the WH side. This implies that in the concentration range $C_{2\beta,w} < C_1 < C_{2\beta,s}$ there is a morphological selection as only fibrils with two WH surfaces can grow, whereas the ones with two SH cannot (see Figure 1). The values for $C_{2\beta,w} = 2.7 \times 10^{22}$ m^{-3} (= 45 mM) and $C_{2\beta,s} = 4.4 \times 10^{22}$ m^{-3} (= 74 mM) are obtained from eqs 5 and 6. In Figure 4d we also show the corresponding $J(C_1)$ dependence for the symmetric case, which shows that the main effect of increasing the asymmetry (decreasing ψ_w at constant ψ_s) is to shift $C_{1\beta}$ to higher concentration and to hamper protein fibrillation, because metanucleation commences at higher C_1 values. Using the C_e values calculated above in eq 14, the threshold concentrations for fibrils with asymmetry ratios 0.5 is $C_{1\beta} = 7.3 \times 10^{22}$ m^{-3} (= 121 mM). A solution mixture containing fibrils with two strong, two weak, and one strong and one weak hydrophobic surface can only be observed at concentrations in the metanucleation regime of all fibrils, i.e. when $C_1 > C_{1\beta} = 121$ mM provided the magnitude of the metanucleation rates are comparable and sufficiently high (see Figure 4d). Note that although the effect of asymmetry is due to changes in the hydrophobicity (as in the case of the conformational change from an extended β-strand to a hairpin), the shift of C_e to higher concentrations does not compensate the corresponding shift of $C_{1\beta}$ to lower ones. This is so, because a change in α_w also changes ψ (see eq 3), which is not the case when the conformation changes from an extended β-strand to a hairpin. The effect of asymmetry on the $J(C_1)$ dependence provides new insight into how a change in the side-chain side-chain interactions between the β-strands can lead to a change in the stacking of β-sheets within fibrils (7).

DISCUSSION

Fibrils solubility and polymorphism

The results obtained highlight the important role of the threshold concentration $C_{1\beta}$ and the fibril solubility C_e in amyloid fibril nucleation, and they illustrate that C_e is the determining factor because $C_{1\beta}$ depends on C_e (eq 14). Describing the phenomenon of fibril polymorphism on the basis of fibril solubility C_e and the threshold concentration $C_{1\beta}$ provides an alternative view on this important problem, and it opens new ways to control the formation of particular fibril polymorphs experimentally by changing $C_{1\beta}$ and C_e. Therefore we express both quantities in terms of the binding energies between neighbouring β-strands in the fibril. An approximate relation between C_e and the binding energies can be obtained by substitution of eqs 1 to 3 into eq 16. This gives

$$C_e = C_r \exp\left[-(n\varepsilon + c_s n_s \varepsilon_s + c_w n_w \varepsilon_w + n_s \varepsilon_s / 2 + n_w \varepsilon_w / 2)/kT\right] \quad (17)$$

where ε, ε_s, and ε_w are the binding energies between nearest neighbour amino acids due to hydrogen bonding and to strong and weak hydrophobic bonds, respectively. The n's are the corresponding number of these bonds, and c_s, c_w are parameters determining the contributions of hydrophobicity-mediated bonds. Similarly, the dependence of $C_{1\beta}$ on the binding energies is obtained by substitution of eqs 1, 2 and 17 into eq 1

$$C_{1\beta} = C_r \exp\left[-(n\varepsilon + c_s n_s \varepsilon_s + c_w n_w \varepsilon_w)/kT\right] \quad (18)$$

These two relatively simple equations allow us to understand and rationalize the results obtained for the concentration dependence of the nucleation rate for different fibril polymorphs in terms of changes in the binding energies. First we consider the conformational polymorphism due to an increase of the β-strand length within fibrils. Figures 3a and 4a illustrate that increasing the β-strand length decreases C_e and promotes protein fibrillation because $C_{1\beta}$ is shifted to much lower C_1 values. The reason for this is that increasing the β-strand length increases n, n_s and n_w, which decreases both C_e and $C_{1\beta}$ (eqs 17 and 18). As ε is ten times larger than ε_s and ε_w, however, this decrease is dominated by the increase in the binding energy due to hydrogen bonds. Second, we consider the packing polymorphism due to parallel or anti-parallel stacking of β-strands in a β-sheet. Figures 3c and 4c illustrate that a change in the stacking of the β-strands in a β-sheet from parallel to antiparallel increases both C_e, $C_{1\beta}$ and thereby hampers protein fibrillation. This decrease is solely due to the decrease in the hydrogen bonding energy, as a change in the stacking arrangement only lowers ε, whereas ε_s and ε_w are unchanged (see eqs 17 and 18). Third, we consider the conformational polymorphism due to a change in the conformation of the β-strand from extended to hairpin. Figures 3b and 4b illustrate that this conformational change only increases C_e, whereas $C_{1\beta}$ is unchanged and consequently protein fibrillation is only slightly hampered. As this conformational change only decreases the numbers n_s, n_w of hydrophobic contacts between β-strands in consecutive β-sheets (and not n), this effect is entirely due a change in the hydrophobic binding energy (see eqs 17 and 18). Forth, we consider the packing polymorphism due to the asymmetry between the weak and strong hydrophobic β-strand surfaces that can lead to different packing of β-sheets within fibrils. Figures 3d and 4d show that increasing the asymmetry increases both C_e and $C_{1\beta}$ thereby hampering protein fibrillation. This effect is also entirely due to an decrease in the hydrophobic binding energy between β-strands as with increasing asymmetry only ε_w is lowered, whereas ε and ε_s are unchanged (see eqs 17 and 18). The morphological selection between fibrils with two WH and SH β-sheet surfaces occurs thanks to the inequality $C_{2\beta,w} < C_{2\beta,s}$, and by substitution of eqs 1, 2 and 17 into eqs 5 and 6 it can be shown that this inequality is due to the fact that $\varepsilon_w < \varepsilon_s$.

General rule

The considerations of these four examples reveal a general rule underlying fibril polymorphism, namely that changes in the conformation of the fibril building blocks or their packing that increase their binding energy within fibrils (due to both hydrogen and hydrophobic bonds) lowers the fibril solubility C_e and hence the threshold

concentration $C_{1\beta}$ which in turn promotes protein fibrillation. Or in other words, the nucleation rate of the fibril polymorphs composed of fibril building blocks with higher binding energy is higher. Although this rule seems intuitive, here we show that it naturally emerges by treating the nucleation of amyloid fibrils into polymorphic structures within our newly developed non-standard nucleation. The power of the presented theoretical framework is that it provides a tool to both qualitatively and quantitatively predict which polymorph forms based on the fundamental interactions between the fibril building blocks.

Limitations

Finally, we emphasize that the results obtained above apply to one-step fibril nucleation, i.e when the monomeric β-strands polymerize directly into fibrils, and that the analysis treats homogeneous nucleation of amyloid fibrils occurring when nucleation-active foreign particles or substrates are absent from the solution. Two-step nucleation of polymorphic fibrils, and fibril polymorphism that occurs during fibril growth, or is determined by fibril growth, are not considered. Importantly, the application of the general expressions for the fibril nucleation rate J as an explicit function of the concentration to different fibril polymorphs requires that the reference concentration C_r and the attachment frequency k_e of monomers to one of the two fibril ends at equilibrium are constant. Furthermore, the relation between the fibril solubility and the binding energies is approximate and pertains to sufficiently low temperatures. It should also be mentioned that the entropy loss when a β-strand is attached to the fibril is taken into account in our newly developed non-standard nucleation model (30, 49). This is so, because in contrast to classical nucleation theory, in the derivation of the analytical expression for the nucleation rate, the length distribution of fibril nuclei in the solution is considered (see Figure 3 of Ref. (30)). The remarkably good description of simulation data for the nucleation rate by our so-derived expression (see Figure 5 of Ref. (30)) indicates that entropy effects is indeed well accounted for. Such effects, however, due to vibrations of the β-strand within fibrils are not explicitly considered, but ideas of how to do that can be found in Ref. (62) and they could be the basis of an important extension of our model. The entropic effects, however, are automatically accounted for when experimental data for C_e and ψ, ψ_h are used.

CONCLUSIONS

Summing up, we conclude that the nucleation of polymorphic amyloid fibrils can be treated within our newly developed non-standard nucleation theory. This treatment allows the prediction of the $J(C_1)$ dependence for different fibril polymorphs, which highlights the important role of the threshold monomer concentration $C_{1\beta}$ and the protein solubility C_e. The focus of experimental studies on amyloids is often on their structure, assembly mechanism and their interactions with the biological environment. Not so many experiments focus on determining the fibril solubility and how it changes with the fibril structure and amino acid sequence. Describing the phenomenon of fibril polymorphism on the basis of fibril solubility C_e and the threshold concentration $C_{1\beta}$ opens up new ways to design experimental strategies to stimulate or prevent the formation of particular fibril polymorphs, and for this our

approximate relations between C_e , $C_{1\beta}$ and the binding energies between neighbouring β-strands in the fibril (eqs 17 and 18) might prove a valuable tool.

ACKNOWLEDGEMENT

The author thanks Dr Leandro Rizzi and Professor Dimo Kashchiev for stimulating discussions during the course of this study and for their comments on the manuscript.

REFERENCES

1. Chiti, F., and C.M. Dobson. 2006. Protein misfolding, functional amyloid, and human disease. *Annu Rev Biochem* 75:333-366.
2. Knowles, T.P.J., and M.J. Buehler. 2011. Nanomechanics of functional and pathological amyloid materials. *Nat Nanotechnol* 6(8):469-479.
3. Tycko, R. 2006. Molecular structure of amyloid fibrils: insights from solid-state NMR. *Q Rev Biophys* 39(1):1-55.
4. Faendrich, M., J. Meinhardt, and N. Grigorieff. 2009. Structural polymorphism of Alzheimers Ab and other amyloid fibrils. *Prion* 3(2):5.
5. Tycko, R. 2014. Physical and structural basis for polymorphism in amyloid fibrils. *Protein Sci* 23(11):1528-1539.
6. Volpatti, L.R., Vendruscolo, M., Dobson, C.M., and Knowles, T.P.J. 2013 A Clear View of Polymorphism, Twist, and Chirality in Amyloid Fibril Formation. *Acs Nano* 7(12):10443-10448.
7. Sawaya, M.R., S. Sambashivan, R. Nelson, M.I. Ivanova, S.A. Sievers, et al. 2007. Atomic structures of amyloid cross-beta spines reveal varied steric zippers. *Nature* 447(7143):453-457.
8. Usov, I., Adamcik, J., and Mezzenga, R. 2013. Polymorphism Complexity and Handedness Inversion in Serum Albumin Amyloid Fibrils. *Acs Nano* 7(12):10465-10474.
9. Fitzpatrick, A.W.P., Debelouchina, G. T., Bayro, M. J., Clare, D. K.,Caporini, M. A., *et al.* 2013. Atomic structure and hierarchical assembly of a cross-beta amyloid fibril. *P Natl Acad Sci USA* 110(14):5468-5473.
10. Sachse, C., M. Fandrich M, and N. Grigorieff. 2008. Paired beta-sheet structure of an A beta(1-40) amyloid fibril revealed by electron microscopy. *P Natl Acad Sci USA* 105(21):7462-7466.
11. Petkova, A.T., et al. 2005. Self-propagating, molecular-level polymorphism in Alzheimer's beta-amyloid fibrils. *Science* 307(5707):262-265.
12. Paravastu, A.K., R.D. Leapman, W.M. Yau WM, and R. Tycko. 2008. Molecular structural basis for polymorphism in Alzheimer's beta-amyloid fibrils. *P Natl Acad Sci USA* 105(47):18349-18354.
13. Qiang, W., Yau, W.M., Luo, Y.Q., Mattson, M.P., and Tycko, R. 2012. Antiparallel beta-sheet architecture in Iowa-mutant beta-amyloid fibrils. *P Natl Acad Sci USA* 109(12):4443-4448.
14. Heise, H., W. Hoyer, S. Becker, O.C. Andronesi, O. C., D. Riedel, D., et al. 2005. Molecular-level secondary structure, polymorphism, and dynamics of full-length alpha-synuclein fibrils studied by solid-state NMR. *P Natl Acad Sci USA* 102(44):15871-15876.
15. Jones, E.M., and W.K. Surewicz. 2005. Fibril conformation as the basis of species- and strain-dependent seeding specificity of mammalian prion amyloids. *Cell* 121(1):63-72.

16. Krishnan, R., and S.L. Lindquist. 2005. Structural insights into a yeast prion illuminate nucleation and strain diversity. *Nature* 435(7043):765-772.
17. Dzwolak, W., V. Smirnovas, R. Jansen, and R. Winter. 2004. Insulin forms amyloid in a strain-dependent manner: An FT-IR spectroscopic study. *Protein Sci* 13(7):1927-1932.
18. Eichner, T., and S.E. Radford. 2011. A Diversity of Assembly Mechanisms of a Generic Amyloid Fold. *Mol Cell* 43(1):8-18.
19. Lu, J.X., Qiang, W., Yau, W. M., Schwieters, C. D., Meredith, S. C.*, et al.* 2013. Molecular Structure of beta-Amyloid Fibrils in Alzheimer's Disease Brain Tissue. *Cell* 154(6):1257-1268.
20. Collinge, J., and A. R. Clarke. 2007. A general model of prion strains and their pathogenicity. *Science* 318(5852):930-936.
21. Diaz-Avalos, R., C.Y. King, J. Wall, M. Simon, and D.L.D. Caspar. 2005. Strain-specific morphologies of yeast prion amyloid fibrils. *P Natl Acad Sci USA* 102(29):10165-10170.
22. Tycko, R., K.L. Sciarretta, J.P.R.O. Orgel, and S.C. Meredith. 2009. Evidence for Novel beta-Sheet Structures in Iowa Mutant beta-Amyloid Fibrils. *Biochemistry-Us* 48(26):6072-6084.
23. Hoyer, W.*,* et al. 2002. Dependence of alpha-synuclein aggregate morphology on solution conditions. *J Mol Biol* 322(2):383-393.
24. Klement, K.*,* et al. 2007. Effect of different salt ions on the propensity of aggregation and on the structure of Alzheimer's A beta(1-40) amyloid fibrils. *J Mol Biol* 373(5):1321-1333.
25. Pedersen, J.S.*,* et al. 2006. The changing face of glucagon fibrillation: Structural polymorphism and conformational imprinting. *J Mol Biol* 355(3):501-523.
26. Paravastu, A.K., Qahwash, I., Leapman, R.D., Meredith, S.C., Tycko R (2009) Seeded growth of beta-amyloid fibrils from Alzheimer's brain-derived fibrils produces a distinct fibril structure. *P Natl Acad Sci USA* 106(18):7443-7448.
27. Makarava, N., and I.V. Baskakov. 2008 The same primary structure of the prion protein yields two distinct self-propagating states. *J Biol Chem* 283(23):15988-15996.
28. Knowles, T.P.J., Shu, W. M., Devlin, G. L., Meehan, S., Auer, S.*, et al.* 2007 Kinetics and thermodynamics of amyloid formation from direct measurements of fluctuations in fibril mass. *P Natl Acad Sci USA* 104(24):10016-10021.
29. Lomakin, A., Chung, D.S., Benedek, G.B., Kirschner, D.A., and Teplow, D.B. 1996. On the nucleation and growth of amyloid beta-protein fibrils: Detection of nuclei and quantitation of rate constants. *P Natl Acad Sci USA* 93(3):1125-1129.
30. Kashchiev, D., R. Cabriolu, and S. Auer. 2013. Confounding the Paradigm: Peculiarities of Amyloid Fibril Nucleation. *J Am Chem Soc* 135(4):1531-1539.Kashchiev D, Cabriolu R, & Auer S (2013) Confounding the Paradigm: Peculiarities of Amyloid Fibril Nucleation. *J Am Chem Soc* 135(4):1531-1539.
31. Auer, S., Ricchiuto, P., and Kashchiev, D. 2012. Two-Step Nucleation of Amyloid Fibrils: Omnipresent or Not? *J Mol Biol* 422(5):723-730.
32. Cohen, S.I.A., Linse, S., Luheshi, L. M., Hellstrand, E., White, D. A.*, et al.* 2013. Proliferation of amyloid-beta 42 aggregates occurs through a secondary nucleation mechanism. *P Natl Acad Sci USA* 110(24):9758-9763.

33. Chiti, F., M. Stefani, N. Taddei, G. Ramponi, and C.M. Dobson. 2003. Rationalization of the effects of mutations on peptide and protein aggregation rates. *Nature* 424(6950):805-808.
34. Fernandez-Escamilla, A.M., F. Rousseau, J. Schymkowitz, and L. Serrano. 2004. Prediction of sequence-dependent and mutational effects on the aggregation of peptides and proteins. *Nat Biotechnol* 22(10):1302-1306.
35. Trovato, A., F. Chiti, A. Maritan, and F. Seno. 2006. Insight into the structure of amyloid fibrils from the analysis of globular proteins. *Plos Comput Biol* 2(12):1608-1618.
36. Tartaglia, G.G., et al. 2008. Prediction of aggregation-prone regions in structured proteins. *J Mol Biol* 380(2):425-436.
37. Morris, A.M., M.A. Watzky, and R.G. Finke. 2009 Protein aggregation kinetics, mechanism, and curve-fitting: A review of the literature. *Bba-Proteins Proteom* 1794(3):375-397.
38. Cohen, S.I.A., M. Vendruscolo, C.M. Dobson, and T.P.J. Knowles. 2012. From Macroscopic Measurements to Microscopic Mechanisms of Protein Aggregation. *J Mol Biol* 421(2-3):160-171.
39. Berryman, J.T., S.E. Radford, and S.A Harris. 2011. Systematic Examination of Polymorphism in Amyloid Fibrils by Molecular-Dynamics Simulation. *Biophys J* 100(9):2234-2242.
40. Miller, Y., B.Y. Ma, and R. Nussinov. 2009. Polymorphism of Alzheimer's A beta(17-42) (p3) Oligomers: The Importance of the Turn Location and Its Conformation. *Biophys J* 97(4):1168-1177.
41. Wei, G.H., A.I. Jewett, and J.E. Shea. 2010. Structural diversity of dimers of the Alzheimer amyloid-beta(25-35) peptide and polymorphism of the resulting fibrils. *Phys Chem Chem Phys* 12(14):3622-3629.
42. Berhanu, W.M., and U.H.E. Hansmann. 2012. Structure and Dynamics of Amyloid-beta Segmental Polymorphisms. *Plos One* 7(7):e41479.
43. Nguyen, P.H., and P. Derreumaux. 2013. Conformational Ensemble and Polymorphism of the All-Atom Alzheimer's A beta(37-42) Amyloid Peptide Oligomers. *J Phys Chem B* 117(19):5831-5840.
44. Pellarin, R., P. Schuetz, E. Guarnera, and A. Caflisch. 2010. Amyloid Fibril Polymorphism Is under Kinetic Control. *J Am Chem Soc* 132(42):14960-14970.
45. Abraham, F.F. 1974. *Homogeneous Nucleation Theory* (Academic, New York).
46. Kashchiev, D. 2000. *Nucleation: Basic Theory with Applications* (Butterworth-Heinemann, Oxford).
47. Cabriolu, R., D. Kashchiev, and S. Auer. 2012. Breakdown of nucleation theory for crystals with strongly anisotropic interactions between molecules. *J Chem Phys* 137(20):204903.
48. Bingham, R.J., L.G. Rizzi, R. Cabriolu, and S. Auer. 2013. Communication: Non-monotonic supersaturation dependence of the nucleus size of crystals with anisotropically interacting molecules. *J Chem Phys* 139(24):241101.
49. Auer, S. 2014. Amyloid Fibril Nucleation: Effect of Amino Acid Hydrophobicity. *J Phys Chem B* 118(20):5289-5299.
50. Perutz, M.F. 1999. Glutamine repeats and neurodegenerative diseases: molecular aspects. *Trends Biochem Sci* 24(2):58-63.
51. Kashchiev, D., and S. Auer. 2010. Nucleation of amyloid fibrils. *J Chem Phys* 132(21):215101.

52. Cabriolu, R., D. Kashchiev, and S. Auer. 2010. Atomistic theory of amyloid fibril nucleation. *J Chem Phys* 133(22):225101.
53. Cabriolu, R., and Auer, S. 2011. Amyloid Fibrillation Kinetics: Insight from Atomistic Nucleation Theory. *J Mol Biol* 411(1):275-285.
54. Kodali, R., Williams, A.D., Chemuru, S., and Wetzel, R. 2010 Abeta(1-40) Forms Five Distinct Amyloid Structures whose beta-Sheet Contents and Fibril Stabilities Are Correlated. *J Mol Biol* 401(3):503-517.
55. Auer, S. and D. Kashchiev. 2010. Phase Diagram of alpha-Helical and beta-Sheet Forming Peptides. *Phys Rev Lett* 104(16):168105.
56. Auer, S. 2011. Phase diagram of polypeptide chains. *J Chem Phys* 135(17):175103.
57. Haas, C., and J. Drenth. 1995. The Interaction Energy between 2 Protein Molecules Related to Physical-Properties of Their Solution and Their Crystals and Implications for Crystal-Growth. *J Cryst Growth* 154(1-2):126-135.
58. Masino, L., and A. Pastore. 2001. A structural approach to trinucleotide expansion diseases. *Brain Res Bull* 56(3-4):183-189.
59. Fersht, A.R., Shi, J. P., Knilljones, J., Lowe, D. M., Wilkinson, A. J.*, et al.* 1985 Hydrogen-Bonding and Biological Specificity Analyzed by Protein Engineering. *Nature* 314(6008):235-238.
60. Nguyen, H.D., and Hall, C.K. 2004 Molecular dynamics simulations of spontaneous fibril formation by random-coil peptides. *P Natl Acad Sci USA* 101(46):16180-16185.
61. Aggeli, A.*,* et al. 2001 Hierarchical self-assembly of chiral rod-like molecules as a model for peptide beta-sheet tapes, ribbons, fibrils, and fibers. *P Natl Acad Sci USA* 98(21):11857-11862.
62. Ferrone, F.A. 2006 Nucleation: the connections between equilibrium and kinetic behavior. *Methods in enzymology* 412:285-299.